Superconducting Magnetic Energy Storage for Pulsed Power Magnet Applications

Ashish Bhardwaj, *Senior Member, IEEE*, Linh N. Nguyen, Josef B. Schillig, Peter Cheetham, *Member, IEEE*, Chul H. Kim, *Senior Member, IEEE*, Doan N. Nguyen, and Sastry Pamidi, *Senior Member, IEEE*

***Abstract*—As part of the exploration of energy efficient and versatile power sources for future pulsed field magnets of the National High Magnetic Field Laboratory-Pulsed Field Facility (NHMFL-PFF) at Los Alamos National Laboratory (LANL), the feasibility of superconducting magnetic energy storage (SMES) for pulsed-field magnets and other pulsed power loads is examined. Basic SMES parameters needed to power one of the coil groups of the large 100 T magnet were determined. A circuit topology for the power transfer between the SMES and the magnet was devised, and the basic performance of the topology was simulated to reproduce the pulse shape currently used in the 100 T magnet. The Finite element analysis (FEA) method was used to calculate the magnetic field distribution of several preferred coil configurations for effective SMES design. Magnetic field distribution and the field dependent critical current density of commercial high temperature superconducting (HTS) tapes were used to understand the conductor/cable requirements for the SMES.**

***Index Terms*—SMES, HTS, FEA, solenoid coil, voltage source converter and power supplies system.**

I. Introduction

SUPERCONDUCTING magnetic energy storage (SME) has been considered for a variety of applications including high-energy physics, high-energy lasers, power quality improvement of the power grid, backup power, and electric transportation [1], [2], [3], [4], [5], [6]. SMES devices store electromagnetic energy in the superconducting inductor and release the stored energy when required [7], [8]. Unlike many other energy storage technologies, SMES is suitable for high power applications because of its fast charge and discharge capabilities [9], [10].

Manuscript received 13 November 2022; revised 5 February 2023; accepted 20 March 2023. Date of publication 11 April 2023; date of current version 28 April 2023. This work was supported in part by the NSF under Cooperative Agreement DMR-1644779 and the State of Florida at the NHMFL-PFF (also known as MPA-MAGLAB) in Los Alamos, NM, USA, and in part by the Office of Naval Research. *(Corresponding author: Ashish Bhardwaj.)*

Ashish Bhardwaj is with the Los Alamos National Laboratory, Los Alamos, NM 87545 USA, and also with the FAMU-FSU College of Engineering and the Center for Advanced Power Systems, Tallahassee, FL 32310 USA (e-mail: ashish@lanl.gov).

Linh N. Nguyen, Josef B. Schillig, and Doan N. Nguyen are with the Los Alamos National Laboratory, Los Alamos, NM 87545 USA (e-mail: linh@lanl.gov; jschillig@lanl.gov; doan@lanl.gov).

Peter Cheetham and Sastry Pamidi are with the FAMU-FSU College of Engineering and the Center for Advanced Power Systems, Tallahassee, FL 32310 USA (e-mail: cheetham@caps.fsu.edu; pamidi@eng.famu.fsu.edu).

Chul H. Kim is with the Center for Advanced Power Systems, Tallahassee, FL 32310 USA (e-mail: ckim@caps.fsu.edu).

Color versions of one or more figures in this article are available at https://doi.org/10.1109/TASC.2023.3265620.

Digital Object Identifier 10.1109/TASC.2023.3265620

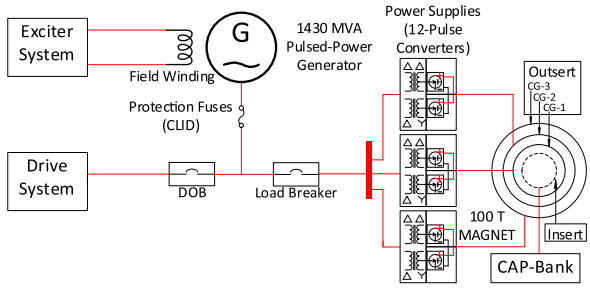

Fig. 1. System block diagram of the 100 T magnet power system.

The interest and possibilities of SMES have increased as the availability of high performance HTS conductors and cables that support the operation at high temperatures without the need for liquid helium, a scarce resource [11]. The advantages of SMES devices compared to other energy storage devices include high energy density, high efficiency, and long life [6], [10], [12].

The 100 T multi-shot magnet is a signature user magnet of the NHMFL-PFF, a national user facility at LANL [13], [14], [15]. Fig. 1 shows a simplified power system block diagram of the 100 T magnet. The 100 T magnet consists of two sets of coils, an insert coil and several outsert coils [14], [15]. The outsert of the magnet consists of 3 coil groups (CG) and these CG are presently powered by the 1430 MVA motor-generator system [15], [16]. The 100 T field pulse is approximately 2.5 s long and requires the coordinated firing of seven 64 MW 12-pulse power converters [14], [15], [16], [17] to create the desired platform field in the outsert. The work on SMES discussed in this paper is focused on the CG-1 of the 100 T outsert. CG-1 has a self-inductance of 26.5 mH and is currently operated at 6 kV with a peak current of 14.5 kA [14], [17].

Besides pulsed magnets, other pulsed loads such as lasers require specific high power pulse shapes [18], [19], [20]. The results of this study and the preliminary design of the SMES for powering the pulsed magnet are relevant for other pulsed load applications.

II. Energy Requirement Calculation

A SMES stores energy in the magnetic field generated by a superconducting inductor. The current in a SMES, an ideal inductor, will remain flowing in persistent mode due to its zero resistance below the critical temperature. The stored energy E of a SMES coil with inductance L and current I can be

1051-8223 © 2023 IEEE. Personal use is permitted, but republication/redistribution requires IEEE permission.
See https://www.ieee.org/publications/rights/index.html for more information.

Authorized licensed use limited to: Florida State University. Downloaded on October 02,2023 at 18:32:18 UTC from IEEE Xplore. Restrictions apply.

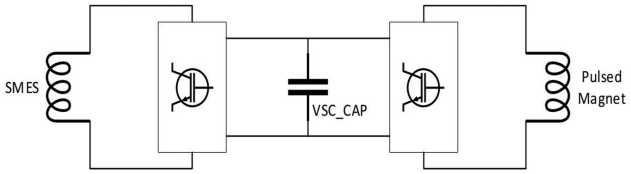

Fig. 2. Simplified electrical circuit.

expressed as

$$E = \frac{1}{2} LI^2 \tag{1}$$

Fig. 2 shows a simplified electrical circuit for connecting the SMES with a pulsed field magnet. This circuit was used to develop a MATLAB Simulink model as shown in Fig. 3 to assess the feasibility of effective energy transfer from the SMES to the pulsed field magnet load. The SMES side H-bridge was controlled to maintain the constant voltage (about 6 kV) across the linked capacitor "VSC_CAP" in the "back-to-back" voltage source converter topology [21], [22], while the pulsed magnet side H-bridge was controlled to have the magnet current follow a prescribed current profile. The SMES side H-bridge was designed to operate in PWM mode, while the magnet side bridge was designed to operate as a voltage reversing switch. Energy flow in both bridges was bi-directional. Both bridges supported the needed persistent/freewheel modes. For long term energy storage, a separate persistent switch across the SMES is needed.

Several SMES designs with different stored energy and operating currents were analyzed. The results indicated, that a SMES with an inductance of 100 mH and stored energy of 45 MJ at 30 kA current would be suitable to pulse the CG-1 and could produce a current waveform very similar to that generated by the currently used power supply system (Fig. 4) [14], [15]. In the current design, the 1430 MVA motor-generator and two series 12-pulse power converters ensure that the total pulse duration of the CG-1 is approximately 200 ms with a flat top of 20 ms. The "CG-1 Current Operational" curve in Fig. 4 shows the pulse shape in the CG-1 used in the operations. The notch seen in the flat top portion of the pulse is due to the firing of the capacitor bank which powers the insert coil. To accomplish the same pulse current shape, the IGBTs are fired using the sequence described in Table I and the abbreviations of different terms are explained in Table II. PM mode ensures the SMES is in energy storage mode, and FW mode ensures that the CG-1 is not open circuited while 100 T pulse is in progress. During CC mode the VSC_CAP is charged to 6 kV, and the Pulse mode ensures the required pulse shape in CG-1.

As shown in Figs. 4, 5, and 6, the energy is effectively transferred and then recovered using two different H-bridges. A similarly controlled current pulse and the corresponding power profile can be fed to the CG-1 using SMES. As shown in Fig. 6, the current in the SMES dropped from 30 kA to around 25.5 kA during the peak field phase of the CG-1 and restored to 29.1 kA at the end of the pulse. Of the about 3.5 MJ of energy delivered to CG-1 at peak field, about 2 MJ were recouped by the SMES at the end of the pulse. Only approximately 1.5 MJ was dissipated during the pulse out of the total 45 MJ stored in SMES prior to the pulse. These simulations suggested that the SMES system, as outlined, could possibly power a few successive pulses prior to needing to be recharged. Simulations also showed that the SMES coil current must always remain higher than ~15 kA, the peak current reached in CG-1 during the pulse.

TABLE I
IGBT FIRING SCHEME

Mode[a]	Switches	SMES S1	SMES S2	SMES S3	SMES S4	Magnet T1	Magnet T2	Magnet T3	Magnet T4
SMES to Magnet									
1	PM & FW	1	0	0	1	0	1	0	1
2	CC & FW	1	1	0	0	0	1	0	1
3	PM & Pulse	1	0	0	1	1	1	0	0
4	CC & Pulse	1	1	0	0	1	1	0	0
Magnet to SMES									
1	PM & CC	1	0	0	1	0	0	1	1
2	SMC & CC	0	0	1	1	0	0	1	1
3	PM & FW	1	0	0	1	0	1	0	1

[a] See Table-II for abbreviations

TABLE II
ABBREVIATIONS

PM	Persistent Mode
FW	Free-Wheel
CC	Capacitor Charging
SMC	SMES Charging

III. SMES MAGNET DESIGN

A. Design Parameters

HTS coils are attractive in SMES applications due to their high current carrying capacity at temperatures > 20 K [3], [4], [5], [23], [24], [25], [26]. Solenoid coil designs are one of the most common topologies for superconducting magnets. They commonly have large stray fields but are nevertheless of great interest due to their simplicity in design and construction. Some groups explored toroidal magnet designs [5], [27], [28], [29] to reduce stray fields. Several optimization schemes were developed for solenoid SMES designs [30], [31], [32], [33]. Hence, a solenoid design is used in this study. We plan to compare the solenoid designs with toroidal designs for SMES magnets in our future studies.

As shown in Fig. 7, the geometry of a solenoid can be defined by the following parameters: inner radius R_i, outer radius R_o, and height H. It can also be defined by the following parameters:

$$\alpha = \frac{R_o}{R_i} \tag{2}$$

$$\beta = \frac{H}{2R_i} \tag{3}$$

There are many different formulae and charts published for the calculation of the inductance of an air-cored solenoid with given dimensions [34], [35], [36], [37]. A more straightforward

Authorized licensed use limited to: Florida State University. Downloaded on October 02,2023 at 18:32:18 UTC from IEEE Xplore. Restrictions apply.

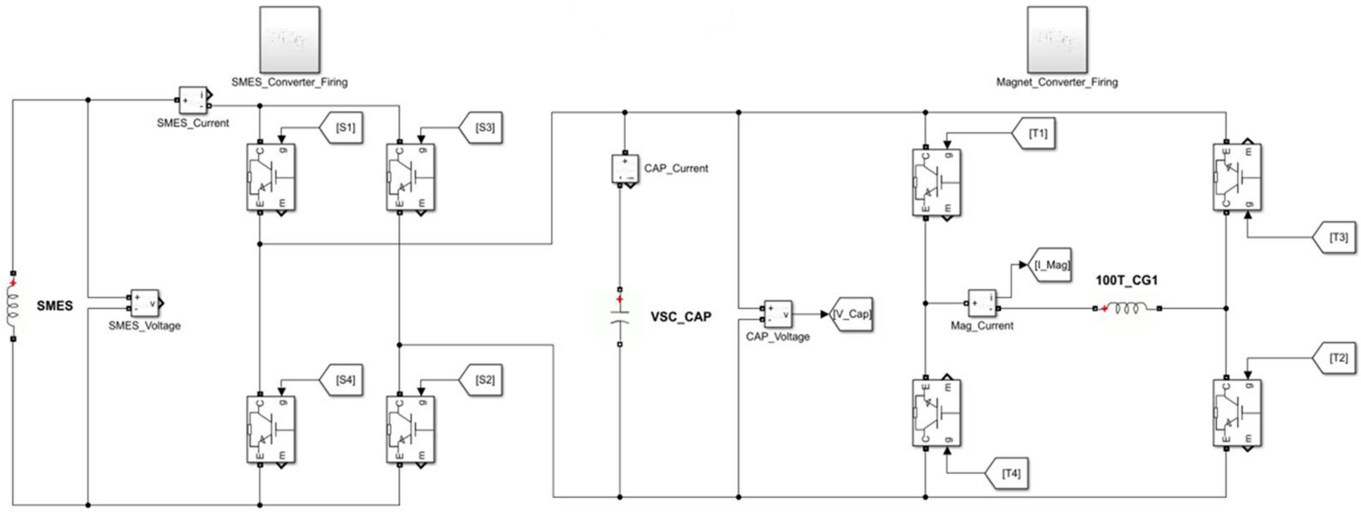

Fig. 3. System block diagram of the 100 T CG-1 power supply.

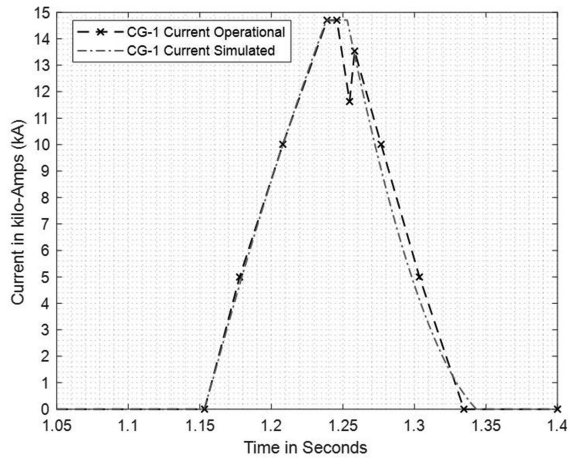

Fig. 4. Operational and simulated current profile comparison of the CG-1 of the 100 T magnet.

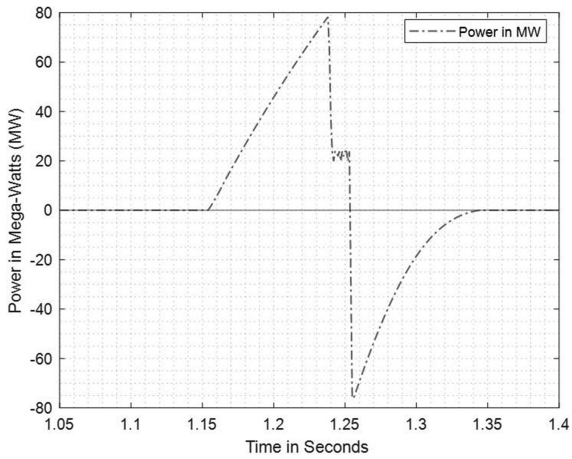

Fig. 5. Power profile of the 100 T CG-1 during each pulse generated by SMES.

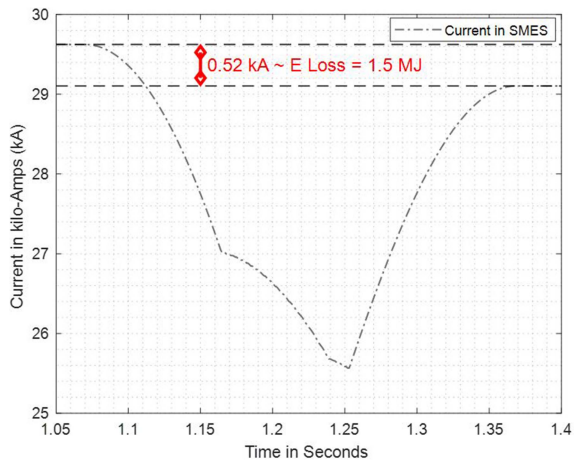

Fig. 6. Discharging and charging the current profile of SMES.

formula was given by Welsby [34] and can be alternatively expressed as follows (where N is the total number of turns):

$$L = f(\alpha, \beta, R_i, N) = \frac{\mu_0 \pi N^2 R_i (\alpha+1)^2}{8\beta} K_n \quad (4)$$

$$K_n = \frac{1}{1 + \frac{0.9(\alpha+1)}{4\beta} + \frac{0.64(\alpha-1)}{(\alpha+1)} + \frac{0.84(\alpha-1)}{2\beta}} \quad (5)$$

B. Minimum Volume Calculation

As the inductance of the SMES coil is known, β can be expressed as the function of L, α, R_i, and A_{cable}. Here A_{cable} = 30 mm x 30 mm is assumed for the area of the cross-section of the HTS cable.

$$x_1 = \left(1 + \frac{0.64(\alpha-1)}{(\alpha+1)}\right) L \quad (6)$$

Authorized licensed use limited to: Florida State University. Downloaded on October 02,2023 at 18:32:18 UTC from IEEE Xplore. Restrictions apply.

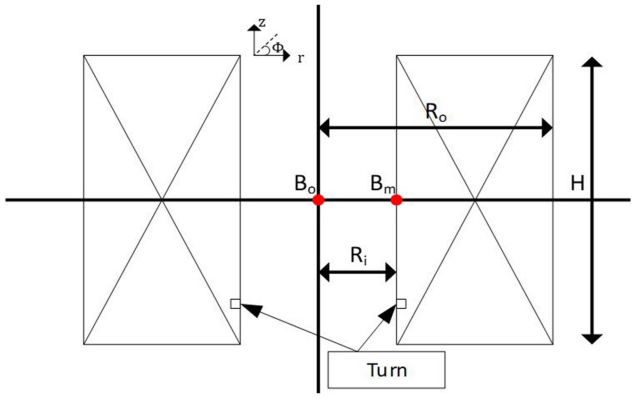

Fig. 7. Cross-sectional view of a solenoid coil.

$$x_2 = \frac{\mu_0 \pi R_i^5 \left(\alpha^2 - 1\right)^2}{A_{cable}^2} \tag{7}$$

$$x_3 = \frac{0.9\,(\alpha + 1)}{4}\, L \tag{8}$$

$$x_4 = \frac{0.84\,(\alpha - 1)}{2}\, L \tag{9}$$

$$\beta = f\,(L, \alpha, R_i, A_{cable}) = \frac{x_1 + \sqrt{x_1^2 + 2x_2\,(x_3 + x_4)}}{x_2} \tag{10}$$

The winding volume of the solenoid can be expressed as below:

$$V_{winding} = 2\pi\beta(\alpha^2 - 1)R_i^3 \tag{11}$$

The total number of turns can be determined by:

$$N = 2\beta\,(\alpha - 1)\,R_i^2/A_{cable} \tag{12}$$

Based on (4) to (12), the winding volume can be expressed as a function of α and R_i or a function of β and R_i. With these functions a minimum winding volume can be calculated for the fixed inductance and the known cable cross-section.

$$V_{winding} = f\ (\alpha, R_i) = g\,(\beta, R_i) \tag{13}$$

Figs. 8 and 9 show the winding volumes as the function of α and β, respectively, for different configurations (α, β, R_i) of the solenoid coil. The bold black line in both figures shows the minimum volume of the winding required for the SMES to store a minimum of 45 MJ. The minimum volume of the winding is found for $\alpha \simeq 2$ and $\beta \simeq 0.5$. This configuration is also known as Brooks coil [37] which generates the highest inductance for a given length of the conductor. In our case, the above observation can be restated as: The minimum volume air core solenoid of fixed inductance and known cable/conductor cross-section area will be a coil with Brooks proportions.

IV. HTS Conductor for SMES Coils

The current carrying capability of a superconductor decreases with increasing applied magnetic field and/or temperature. Hence the total current carrying capacity depends on

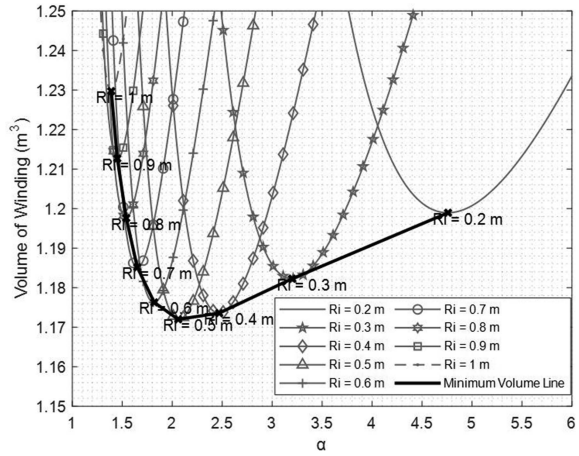

Fig. 8. Winding volume as a function of α.

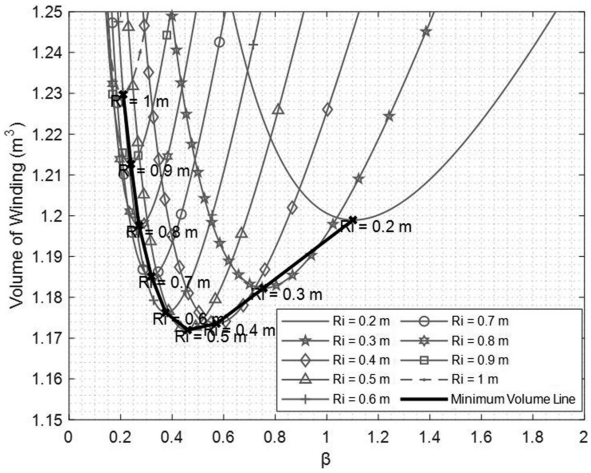

Fig. 9. Winding volume as a function of β.

the maximum field in the windings and the number of HTS tapes in the cable used to wind the coil. To determine the required number of HTS tapes for the HTS cables, the maximum field in the winding must be calculated. For each value of R_i considered, the maximum field value was determined for the respective minimum volume coil geometry using the COMSOL FEA software. Fig. 10 depicts the magnetic field distribution in the lowest volume designs for R_i = 0.4 m, 0.6 m, 0.8 m, and 1 m. The maximum field (B_m) is, as expected, observed at the coil's inner diameter along the mid-plane ($r = R_i$, $z = 0$ m). Fig. 11 is showing the maximum field values for the various R_i considered.

The width of the HTS tape considered for the cable build is 4 mm with a thickness of 0.1 mm. The in-field performance for AP REBCO tapes at several temperatures and other relevant electrical and mechanical parameters shown in Table III were obtained from Superpower-Inc. website [38]. The experimental data of the different temperatures and external transverse field dependence critical currents (I_c vs $B_\perp$) for $B_\perp$>5 T were plotted in Fig. 12, using (14) and the curve fit parameters.

$$I_c = I_0 + Ae^{-kB_\perp} \tag{14}$$

Authorized licensed use limited to: Florida State University. Downloaded on October 02,2023 at 18:32:18 UTC from IEEE Xplore. Restrictions apply.

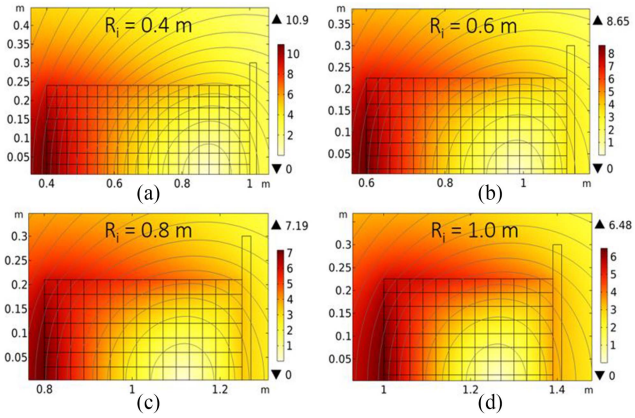

Fig. 10. Magnetic field distribution in different coil configurations.

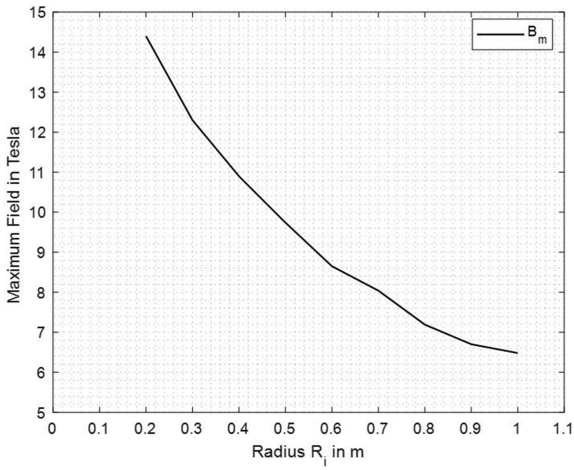

Fig. 11. Maximum field in different coil configurations.

TABLE III
ELECTRICAL AND MECHANICAL PARAMETERS OF SUPERPOWER SCS4050 REBCO TAPE

I_c (77 K, self-field)	120 ~ 160 A/4 mm tape width
I_c (@ different temperature)	Fig.12
Maximum Stress (at 77 K)	> 550 MPa
Minimum bending diameter	11 mm

Given the chosen SMES operating current of 30 kA, I_c of the HTS cable was chosen to be 37.5 kA, ensuring a 25% operating margin. Fig. 13 shows the total HTS tape length required for the different configurations at different operating temperatures discussed above. The fact, that the maximum field B_m ($r = R_i$, $z = 0$ m) was used for $B_\perp$ when using data from Fig. 12, adds, depending on the cable build, an additional margin. The number of tapes needed to reach the desired 37.5 kA capacity of the cable was calculated using the expression below:

$$N_{tapes} = I_{c,cable}/I_{c,tape} \tag{15}$$

With the number of cable-turns of each configuration given by (12) and the cable length l_{cable} calculated from R_i, α, and β, the HTS tape length needed for each of the configurations can

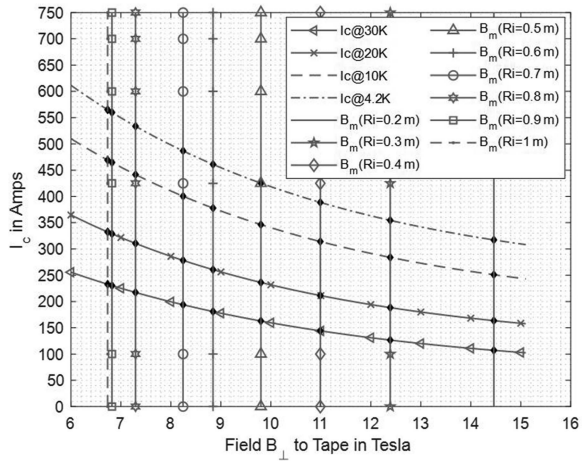

Fig. 12. Critical current as a function of perpendicular field reproduced from [38].

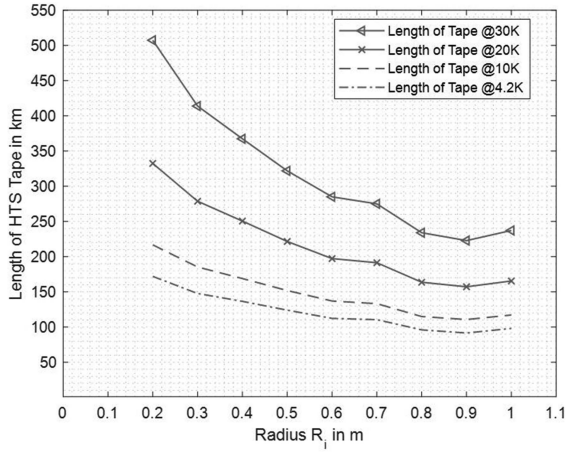

Fig. 13. Tape length for different configurations.

be given by:

$$l_{tape} = l_{cable} * N_{tapes} \tag{16}$$

As can be gleaned from Fig. 13, a 45 MJ SMES coil seems to require the shorter HTS conductor tape length with increasing R_i regardless of the chosen operating temperature.

V. CONCLUSION

The study presented suggests that, in principle, a SMES coil with an about 1.17 m^3 minimum winding volume, operating at 30 kA and stored energy of 45 MJ could, when combined with the described converter topology, reproduce the shape of the current pulse in CG-1 of the 100 T pulsed magnet, which currently is generated using a controlled rectifier set capable of 6.4 kV at 20 kA and powered by LANL's 1430 MVA synchronous motor-generator set. The SMES system topology described can deliver energy to and recover energy from the pulsed magnet as the currently installed system does. The FEA simulations combined with critical current considerations showed that, for fixed energy, increasing the inner radius R_i would lower the maximum magnetic field B_m in the coil as well as lower the

Authorized licensed use limited to: Florida State University. Downloaded on October 02,2023 at 18:32:18 UTC from IEEE Xplore. Restrictions apply.

amount of HTS tape needed to build the coil independent of the operating temperature chosen for the SMES. Our future studies will elaborate on the designs and explore toroidal designs along with the solenoid design reported here.

REFERENCES

[1] J. Rogers et al., "30-MJ superconducting magnetic energy storage (SMES) unit for stabilizing an electric transmission system," *IEEE Trans. Magn.*, vol. 15, no. 1, pp. 820–823, Jan. 1979, doi: 10.1109/TMAG.1979.1060044.

[2] W. Hassenzahl, "A comparison of the conductor requirements for energy storage devices made with ideal coil geometries," *IEEE Trans. Magn.*, vol. 25, no. 2, pp. 1799–1802, Mar. 1989, doi: 10.1109/20.92651.

[3] L. Ren et al., "Development of a movable HTS SMES system," *IEEE Trans. Appl. Supercond.*, vol. 25, no. 4, Aug. 2015, Art. no. 5701109, doi: 10.1109/TASC.2015.2437335.

[4] K. Shikimachi et al., "Development of MVA class HTS SMES system for bridging instantaneous voltage dips," *IEEE Trans. Appl. Supercond.*, vol. 15, no. 2, pp. 1931–1934, Jun. 2005, doi: 10.1109/TASC.2005.849338.

[5] R. Gupta et al., "Design, construction, and testing of a large-aperture high-field HTS SMES coil," *IEEE Trans. Appl. Supercond.*, vol. 26, no. 4, Jun. 2016, Art. no. 5700208, doi: 10.1109/TASC.2016.2517404.

[6] P. D. Baumann, "Energy conservation and environmental benefits that may be realized from superconducting magnetic energy storage," *IEEE Trans. Energy Convers.*, vol. 7, no. 2, pp. 253–259, Jun. 1992, doi: 10.1109/60.136217.

[7] D. Sutanto and K. W. E. Cheng, "Superconducting magnetic energy storage systems for power system applications," in *Proc. IEEE Int. Conf. Appl. Supercond. Electromagn. Devices*, 2009, pp. 377–380, doi: 10.1109/ASEMD.2009.5306614.

[8] B. Kondratowicz-Kucewicz, "The energy and the magnetic field in HTS superconducting magnetic energy storage model," in *Proc. IEEE Int. Conf. Electromagn. Devices Processes Environ. Protection Seminar Appl. Supercond.*, 2017, pp. 1–4, doi: 10.1109/ELMECO.2017.8267757.

[9] K. P. Juengst and H. Salbert, "Fast SMES for generation of high power pulses," *IEEE Trans. Magn.*, vol. 32, no. 4, pp. 2272–2275, Jul. 1996, doi: 10.1109/20.508619.

[10] C. Rey, *Superconductors in the Power Grid: Materials and Applications*. Sawston, Cambridgem USA: Woodhead Publishing, 2015.

[11] Z. S. Hartwig et al., "VIPER: An industrially scalable high-current high-temperature superconductor cable," *Supercond. Sci. Technol.*, vol. 33, no. 11, Oct. 2020, Art. no. 11LT01, doi: 10.1088/1361-6668/abb8c0.

[12] Y. Huang, Y. Ru, Y. Shen, and Z. Zeng, "Characteristics and applications of superconducting magnetic energy storage," *J. Phys.: Conf. Ser.*, vol. 2108, no. 1, Nov. 2021, Art. no. 012038, doi: 10.1088/1742-6596/2108/1/012038.

[13] D. N. Nguyen, J. Michel, and C. H. Mielke, "Status and development of pulsed magnets at the NHMFL pulsed field facility," *IEEE Trans. Appl. Supercond.*, vol. 26, no. 4, Jun. 2016, Art no. 4300905, doi: 10.1109/TASC.2016.2515982.

[14] J. R. Sims, D. G. Rickel, C. A. Swenson, J. B. Schillig, G. W. Ellis, and C. N. Ammerman, "Assembly, commissioning and operation of the NHMFL 100 Tesla multi-pulse magnet system," *IEEE Trans. Appl. Supercond.*, vol. 18, no. 2, pp. 587–591, Jun. 2008, doi: 10.1109/TASC.2008.922541.

[15] J. Sims et al., "First 100 T non-destructive magnet," *IEEE Trans. Appl. Supercond.*, vol. 10, no. 1, pp. 510–513, Mar. 2000, doi: 10.1109/77.828284.

[16] H. J. Boenig, J. B. Schillig, H. E. Konkel, P. L. Klingner, T. L. Petersen, and J. D. Rogers, "Design installation and commissioning of the Los Alamos National Laboratory pulsed power generator," *IEEE Trans. Energy Convers.*, vol. 7, no. 2, pp. 260–266, Jun. 1992, doi: 10.1109/60.136219.

[17] J. B. Schillig et al., "Design and testing of a 320 MW pulsed power supply," in *Proc. IEEE Conf. Rec. Ind. Appl. Conf. Thirty-2nd IAS Annu. Meeting*, vol. 2, 1997, pp. 1600–1607, doi: 10.1109/IAS.1997.629065.

[18] J. F. Holzrichter, D. Eimerl, E. V. George, J. B. Trenholme, W. W. Simmons, and J. T. Hunt, "High power pulsed lasers," *J. Fusion Energy*, vol. 2, no. 1, pp. 5–45, Feb. 1982, doi: 10.1007/bf01052387.

[19] Q. Zhao, S. Li, R. Cao, D. Wang, and J. Yuan, "Design of pulse power supply for high-power semiconductor laser diode arrays," *IEEE Access*, vol. 7, pp. 92805–92812, 2019, doi: 10.1109/ACCESS.2019.2928011.

[20] P. Benin et al., "Pulsed power conditioning system for the megajoule laser," in *Proc. IEEE 28th Int. Conf. Plasma Sci. 13th Int. Pulsed Power Conf.*, 2001, pp. 401–404, doi: 10.1109/PPPS.2001.961086.

[21] R. K.-L. Lian, R. K. Subroto, V. Andrean, and B. H. Lin, "Modeling of voltage source converters," in *Proc. Harmonic Model. Voltage Source Converters Using Basic Numer. Methods*, 2022, pp. 95–147, doi: 10.1002/9781119527190.ch5.

[22] J. M. Carrasco et al., "Power-electronic systems for the grid integration of renewable energy sources: A survey," *IEEE Trans. Ind. Electron.*, vol. 53, no. 4, pp. 1002–1016, Jun. 2006, doi: 10.1109/TIE.2006.878356.

[23] M. Song et al., "100 kJ/50 kW HTS SMES for micro-grid," *IEEE Trans. Appl. Supercond.*, vol. 25, no. 3, Jun. 2015, Art. no. 5700506, doi: 10.1109/TASC.2014.2386345.

[24] S. Kwak et al., "Design of HTS magnets for a 2.5MJ SMES," *IEEE Trans. Appl. Supercond.*, vol. 19, no. 3, pp. 1985–1988, Jun. 2009.

[25] S. Nagaya et al., "Development of high strength pancake coil with stress controlling structure by REBCO coated conductor," *IEEE Trans. Appl. Supercond.*, vol. 23, no. 3, Jun. 2013, Art. no. 4601204, doi: 10.1109/TASC.2012.2233854.

[26] A. Morandi, B. Gholizad, and M. Fabbri, "Design and performance of a 1 MW-5 s high temperature superconductor magnetic energy storage system," *Supercond. Sci. Technol.*, vol. 29, no. 1, Dec. 2015, Art. no. 015014, doi: 10.1088/0953-2048/29/1/015014.

[27] Y. Zhang, Y. Tang, C. Zhang, Z. Xia, and L. Ren, "Performance and analysis of no-insulation HTS toroidal magnet," *IEEE Trans. Appl. Supercond.*, vol. 27, no. 4, Jun. 2017, Art. no. 4201305, doi: 10.1109/TASC.2017.2660582.

[28] A. Morandi, M. Fabbri, B. Gholizad, F. Grilli, F. Sirois, and V. M. R. Zermeño, "Design and comparison of a 1-MW/5-s HTS SMES with toroidal and solenoidal geometry," *IEEE Trans. Appl. Supercond.*, vol. 26, no. 4, Jun. 2016, Art. no. 5700606, doi: 10.1109/TASC.2016.2535271.

[29] S. Lee et al., "Design of HTS toroidal magnets for a 5 MJ SMES," *IEEE Trans. Appl. Supercond.*, vol. 22, no. 3, Jun. 2012, Art. no. 5700904, doi: 10.1109/TASC.2011.2175871.

[30] K. Kaiho, T. Namba, T. Ohara, and K. Koyama, "Optimization of superconducting solenoid," *Cryogenics*, vol. 16, no. 10, pp. 587–588, Oct. 1976, doi: 10.1016/0011-2275(76)90188-0.

[31] Z. X. Feng, "Optimization of superconducting solenoid coil," *IEEE Trans. Magn.*, vol. 24, no. 2, pp. 926–929, Mar. 1988, doi: 10.1109/20.11378.

[32] J.-M. Rey et al., "Geometry optimization for SMES solenoids using HTS ribbons," *IEEE Trans. Appl. Supercond.*, vol. 21, no. 3, pp. 1670–1673, Jun. 2011, doi: 10.1109/TASC.2010.2095402.

[33] R. Wesche, "Optimization studies of solenoidal windings for superconducting magnetic energy storage," *Cryogenics*, vol. 32, no. 6, pp. 578–583, Jan. 1992, doi: 10.1016/0011-2275(92)90044-B.

[34] V. G. Welsby, *The Theory and Design of Inductance Coils*. London, U.K.: Macdonald, 1960.

[35] M. N. Wilson, *Superconducting Magnets*. Oxford, U.K.: Clarendon, 1983.

[36] D. B. Montgomery, *Solenoid Magnet Design*. Hoboken, NJ, USA: Wiley, 1969.

[37] F. W. Grover, *Inductance Calculations*. New York, NY, USA: Dover, 1946.

[38] "2G HTS wire specification | superpower," *SuperPower Inc.*, [Online]. Available: https://www.superpower-inc.com/specification.aspx

Authorized licensed use limited to: Florida State University. Downloaded on October 02,2023 at 18:32:18 UTC from IEEE Xplore. Restrictions apply.